Biochemical Engineering Journal 135 (2018) 123–132

Contents lists available at ScienceDirect

Biochemical Engineering Journal

journal homepage: www.elsevier.com/locate/bej

Regular article

Controlled network structures of chitosan-poly(ethylene glycol) hydrogel microspheres and their impact on protein conjugation

Sukwon Jung[a], Yi Tang[a], Gyurak Shim[b], Chang-Soo Lee[b], Chang-Hyung Choi[c], Hyunmin Yi[a,*]

[a] Department of Chemical and Biological Engineering, Tufts University, Medford, MA, USA
[b] Department of Chemical Engineering, Chungnam National University, Daejeon, Republic of Korea
[c] Division of Cosmetic Science and Technology, Daegu Haany University, Geongsan, Republic of Korea

ARTICLE INFO

Article history:
Received 8 October 2017
Received in revised form 16 April 2018
Accepted 18 April 2018
Available online 22 April 2018

Keywords:
Hydrogel network
Chitosan
Poly(ethylene glycol)
Protein conjugation
Click reaction
Microsphere

ABSTRACT

We demonstrate a facile approach to manufacture hydrogel microspheres with controlled and macroporous network structures via a simple yet versatile micromolding-based technique. Specifically, highly uniform poly(ethylene glycol) (PEG) hydrogel microspheres containing chemically functional chitosan are readily fabricated using the micromolding-based technique that utilizes surface tension-induced droplet formation of aqueous prepolymer solution followed by photo-induced interfacial polymerization. Network structures of the hydrogel microspheres are readily controlled by simple addition of inert porogen, which induces phase separation during the polymerization. Fluorescent labeling studies reveal tunable distribution of the chitosan within the PEG networks (i.e., uniform and core-shell like distributions) depending on the content of the porogen in the prepolymer solution. In addition, protein conjugation studies show tunable pore sizes and 3D network structures by adjusting content of the porogen, and formation of macroporous networks leading to significantly improved protein conjugation kinetics. The macroporous network structures are further supported with scanning electron microscopy (SEM) results that correspond well with confocal microscopy results. We believe that our fabrication strategy offers a simple and robust route to construct diverse 3D hydrogel network structures with chemical functionality, enabling production of a variety of biofunctionalized hydrogel microspheres that can be utilized in various biomedical applications.

1. Introduction

Hydrogel microparticle-based suspension arrays hold significant potential as powerful alternatives to planar and bead-based arrays for medical diagnostic and biosensing applications [1–4]. Specifically, hydrogel microparticles offer several advantages over solid bead-based ones such as solution-like environment for ideal target-probe binding with minimal non-specific adsorption, rapid assay time, and reduced signal to noise ratio by enhanced loading and capture capacity of probes and targets, respectively [4,5]. Recent advances in the fabrication techniques of the hydrogel microparticles have enabled convenient shape-based encoding and rapid production of complex and/or multicompartmental microparticles, opening doors for multiplexed sensing or diagnostic assays. Such techniques include stop-flow lithography [6–8], photolithography [9–11], capillary microfluidics [12–15] and electrohydrodynamic co-jetting [16,17].

Despite such advances, there still exist several critical challenges in simple and programmable fabrication of the hydrogel microparticles with desired properties. First, most current techniques including microfluidic methods require complex equipment and delicate control of microflows and solution properties (e.g., viscosity and surface tension). Second, the most commonly used polymerizable unit poly(ethylene glycol) diacrylate (PEGDA) with low molecular weight is often not suitable for the creation of large pores that permit rapid diffusion and binding of large biomolecular targets [18–21]. Lastly, the common co-polymerization technique to incorporate biomolecular probes (e.g., antibodies) with the hydrogel network faces challenges in preserving their biospecific affinities due to the harsh radical polymerization environment [22–24]. There thus exist critical needs for simple and reliable techniques to produce hydrogel microparticles with controlled and tunable macroporous network structures as well as chemical func-

* Corresponding author.
E-mail address: hyunmin.yi@tufts.edu (H. Yi).

https://doi.org/10.1016/j.bej.2018.04.012
1369-703X/

tionalities that allow for facile and efficient conjugation of the biomolecules.

We recently reported facile fabrication of chemically functional hydrogel microparticles via simple micromolding techniques and incorporation of chitosan [18,25,26]. As shown in the chemical structure in Fig. 1(a), chitosan is a naturally derived aminopolysaccharide that provides abundant and highly reactive primary amines as an efficient conjugation handle due to their low pK_a value [27–29], making it an enabling biofabrication component that imparts potent chemical functionality [30]. With facile post-fabrication biofunctionalization approaches using the primary amines and bioorthogonal conjugation reactions, we demonstrated utilization of the chitosan-incorporated hydrogel microparticles as protein conjugation and biosensing platforms [18,25]. However, there still exist limitations in mass transfer of large biomolecules into the microparticles leading to slow protein conjugation kinetics owing to tightly crosslinked hydrogel networks. Such slow mass transfer leads to longer incubation and assay time, which in turn can cause compromised results on labile biomolecular probes and targets. In addition, imparting a diverse range of 3D network structures including core-shell geometries with tunable shell thicknesses and mesh sizes could open doors for the development of more versatile sensing platforms. For example, such sensing platforms may be suitable for accurate size discrimination and/or detection of larger biomolecular assemblies such as viruses and protein aggregates (e.g., beta amyloid oligomers implicated in Alzheimer's disease or alpha-synuclein in Parkinson's disease) [31,32]. Therefore, it is imperative that more thorough examination of fabrication parameters and routes to impart wider ranges of 3D network structures should be conducted toward potent hydrogel microparticle design and manufacturing principles.

In this report, we demonstrate a simple approach to drastically increase mesh sizes for improved protein conjugation kinetics and to further fine-tune the network structures of hydrogel microspheres, by exploiting inert porogens from crosslinking PEGDA (scheme in Fig. 1(a)) [33,34]. Briefly, aqueous prepolymer solution containing PEGDA, chitosan and inert short chain PEG porogen is added into PDMS molds, and then the prepolymer solution droplets are spontaneously formed by surface tension upon placing hydrophobic wetting fluid on the mold [26,35–37]. The droplets are crosslinked by photo-induced polymerization reaction of PEGDA, while the crosslinked PEG chains create excluded volume by PIPS during the polymerization reaction [26]. The PEG porogens are then simply washed out during rinsing, leaving large pores within the microspheres. Notably, this approach enables facile tuning of 3D network structures (i.e., core-shell like microspheres with different shell thicknesses and mesh sizes) using simple fabrication parameters such as the PEGDA and PEG porogen content, as well as addressing the mass transfer limitation that allows for improvement in protein conjugation. Specifically, addition of the short PEG porogen (MW 600 Da) at varying concentrations (10–30 v/v%) in the prepolymer solution leads to diverse 3D network structures of the resulting hydrogel microspheres and varying distribution of chemical conjugation handles, allowing for programmable biomolecule conjugation profiles within the microspheres. The fluorescent labeling and protein conjugation results show not only tunable network structures but also enhancement in mass transfer and conjugation of large biomolecules into the microspheres, highly desirable for bioassays in practical clinical settings. In-depth characterization via confocal microscopy and SEM further supports the observed tunable 3D network structures that lead to controllable protein conjugation profiles and kinetics, providing deep insights into the detailed structural features of the hydrogel microspheres. These insights should thus offer promising routes to construct hydrogel microscale materials with varying 3D network structures, and lead to a significant advancement toward facile manufacturing

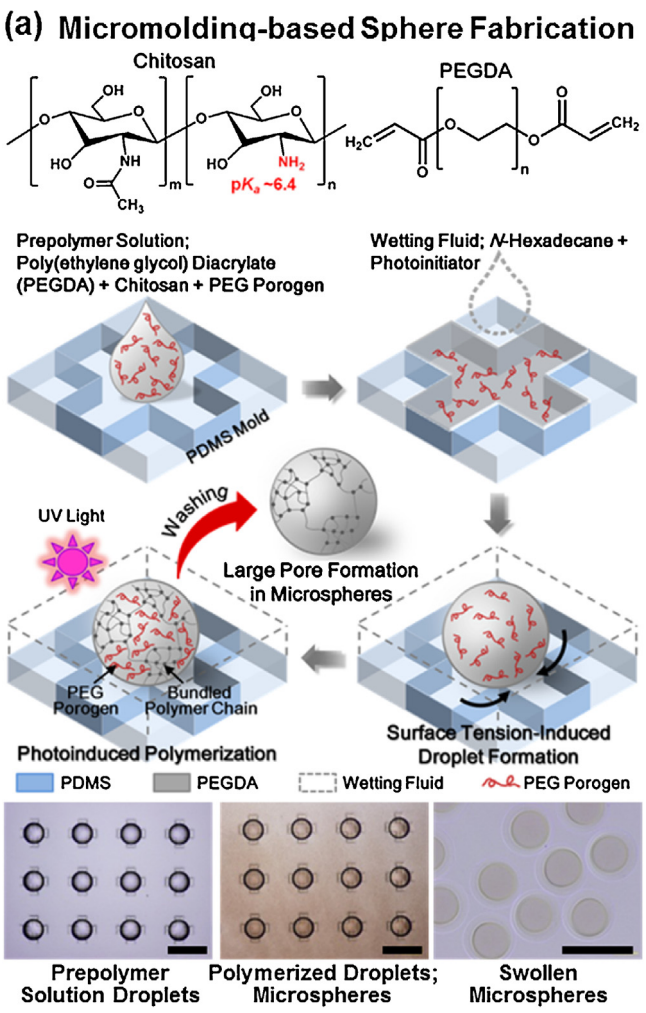

(b) Swelling Capacity of Microspheres

PEGDA (vol%)	PEG600 (vol%)	D_{wet} (μm)	D_{dry} (μm)	Swelling Ratio	Water Content (vol%)
10	0	140±6	81±5	5.2	81
	10	146±5	83±5	5.4	81
	20	148±5	87±6	4.9	80
	30	150±4	89±6	4.9	80
15	0	143±5	89±2	4.2	76
	10	148±5	90±4	4.5	78
	20	151±4	91±4	4.6	78
	30	157±3	92±3	4.9	80

Fig. 1. Fabrication of chitosan–PEG hydrogel microspheres via a simple micromolding-based technique. (a) Chemical structures of main components in prepolymer solution, and schematic diagram describing procedure of the fabrication along with corresponding bright-field micrographs to each step. Scale bars represent 200 μm. (b) Summary of swelling capacity of the as-prepared microspheres ($n \geq 20$).

of potent biofunctionalized microentities for biosensing applications.

2. Materials and methods

2.1. Materials

Chitosan oligosaccharide lactate (average M_n 5 kDa, >90% deacetylation), poly(ethylene glycol) diacrylate (PEGDA, average M_n 700 Da), poly(ethylene glycol) (PEG600, average M_n 600 Da), 2-hydroxy-2-methylpropiophenone (photoinitiator also known as Darocur 1173, PI), and saline sodium citrate (SSC) buffer (20 × concentrate, molecular biology grade) were purchased from Sigma-Aldrich (St. Louis, MO). 5-(and 6-)carboxyfluorescein succinimidyl ester (NHS-fluorescein) was purchased from Pierce Biotechnology (Rockford, IL). Trans-cyclooctene (TCO)–PEG_4–*N*-hydroxysuccinimide (NHS) ester and tetrazine (Tz)–PEG_5–NHS ester were purchased from Click Chemistry Tools (Scottsdale, AZ). Tween 20 (TW20) was purchased from Fisher BioReagents™ (Waltham, MA), poly(dimethylsiloxane) (PDMS) elastomer kits (Sylgard 184) were purchased from Dow Corning (Auburn, MI). Centrifugal filter units (Amicon® Ultra 0.5 ml, EMD Millipore) were purchased from EMD Millipore (Billerica, MA). Dimethyl sulfoxide (DMSO, extra dry) and *N*-hexadecane (99%) were purchased from ACROS Organics™ (Morris, NJ). 2-propanol (>99.7%) was purchased from J.T.Baker® (Center Valley, PA). Red fluorescent protein R-Phycoerythrin (R-PE in sodium phosphate buffer, pH 7.0 with ammonium sulfate) was purchased from AnaSpec (Fremont, CA). All the chemicals were analytical grade, and used without further purification.

2.2. Fabrication of chitosan–PEG hydrogel microspheres

For fabrication of hydrogel microspheres, we utilized a simple micromolding-based technique as in a recent study [26] with minor modifications. Schematic diagram of Fig. 1(a) describes procedure of the microsphere fabrication. Specifically, a PDMS mold consisting of cross-shaped microwells (5.14 nL volume with 297 μm in length and 105 μm in depth) was prepared first, following standard procedure of thermal curing (overnight at 65 °C) of Sylgard 184 elastomer (9:1 wt ratio of elastomer to curing agent) on a silicon master mold with photolithographically patterned cross shapes [11,38]. Prepolymer solutions were prepared by mixing PEGDA (10% v/v or 15% v/v), chitosan (0.5% w/v), PEG600 (0–30% v/v) and deionized (DI) water, and wetting fluid was prepared by mixing 1% v/v of PI with *N*-hexadecane. To fill the microwells with the prepolymer solutions, the as-prepared PDMS mold was covered with the prepolymer solutions and rubbed with a disposable pipet tip. The excess prepolymer solutions were then removed with a pipette, and the filled mold was covered with the wetting fluid. Importantly, this procedure was conducted in a humidity chamber with ~95% humidity in order to minimize loss of water content in the nL volume of the prepolymer solution by rapid evaporation [11]. Next, the mold covered with the wetting fluid was left on an aluminum mirror (Thorlabs, Newton, NJ) for at least 2 min, and the droplets of the prepolymer solution were formed by surface tension at the interface between the prepolymer solution and the wetting fluid. To crosslink the droplets by photo-induced polymerization, 365 nm UV light was irradiated with an 8 W hand-held UV lamp (Spectronics Corp., Westbury, NY) for 5 min. The crosslinked droplets (i.e., microspheres mainly consisting of PEG networks) were then collected by pipetting, and washed 3 times with 2-propanol, 2 times with DI water containing 0.5% v/v TW20 and 3 times with 5 × SSC buffer solution containing 0.05% v/v TW20 (SSC–TW20 buffer solution).

2.3. Measurement of swelling ratio and water content

For the measurement of swelling ratio and water content of the microspheres, we first stored the as-prepared microspheres in SSC–TW20 buffer solution for at least 1 day to reach equilibrium swelling (i.e., wet state). The microspheres were then imaged with the Olympus BX51 microscope (Center Valley, PA) under a bright-field mode, and their diameters (d_{wet}) were measured with an image analysis software ImageJ [39]. To measure diameters of the microspheres under dry state (d_{dry}), lyophilized microspheres were analyzed via SEM (further details in the imaging analysis section below). These diameters under wet and dry state were then utilized to compute the volumetric swelling ratio:

$$\text{Swelling Ratio} = \frac{V_{wet}}{V_{dry}}$$

and water content:

$$\text{Water Content} = \frac{V_{wet} - V_{dry}}{V_{wet}} \times 100\%$$

where V_{wet} and V_{dry} represent sphere volumes under wet and dry states, respectively. To ensure accuracy of the computed swelling ratio and water content, we analyzed at least 20 microspheres per each condition.

2.4. Fluorescent labeling and chemical modification of chitosan–PEG hydrogel microspheres

To label the microspheres with fluorescein dyes via amidation reaction [40], a constant number (~40) of the microspheres were incubated in SSC–TW20 buffer solution with 100 μM of NHS-fluorescein for 1 h at room temperature. To remove unreacted and nonspecifically bound fluorescein molecules, the microspheres were rinsed 3 times with aqueous 2-propanol solution (50% v/v). Similarly, the microspheres were activated with Tz molecules via the same amidation reaction. A constant number (~40) of the microspheres were incubated in SSC–TW20 buffer solution with 500 μM of Tz–PEG_5–NHS ester for 1 h at room temperature, and then the microspheres were washed 5 times with SSC–TW20 buffer solution to remove unreacted chemicals.

2.5. Chemical modification of proteins

To activate R-PEs with TCO molecules, we utilized amidation reaction between lysines of proteins and NHS-ester groups of TCO–PEG_4–NHS ester molecules. For the efficient amidation reaction, we first exchanged buffer solution of the purchased R-PE solution for borate buffered saline buffer solution (50 mM borate, 300 mM NaCl, pH 8.5) via centrifugal filtration at 4 °C (i.e., increase in the pH value) [41]. Next, 2 mg/mL of the R-PEs were incubated with 20-fold molar excess of TCO–PEG_4–NHS ester for 30 min at room temperature. The activated R-PEs were purified from unreacted chemicals via centrifugal filtration (Amicon Ultra 0.5) with PBS buffer solution (pH 7.4) following the manufacturer's standard protocol. Concentrations of the final R-PE solutions were determined by using UV–vis spectrophotometry (EvolutionTM 300 UV–vis Spectrophotometer, Thermo scientific, Waltham, MA) with the characteristic absorbance peaks and molar extinction coefficients of the R-PE ($1.96 \times 10^6\ M^{-1}\ cm^{-1}$ at 565 nm) [42].

2.6. Protein conjugation with microspheres

To conjugate R-PEs with the microspheres and investigate conjugation kinetics, we utilized Tz–TCO ligation reaction; roughly forty Tz-activated microspheres were reacted with 2 μM of TCO-activated R-PEs for varying times (0–24 h) in SSC–TW20 buffer

solution at room temperature. To remove unconjugated R-PEs, the microspheres were washed 5 times with SSC–TW20 buffer solution.

2.7. Imaging analysis

The fluorescently labeled and R-PE conjugated microspheres were imaged with an epifluorescence microscope (Olympus BX51 equipped with a DP70 microscope digital camera, Center Valley, PA) and a confocal microscope (Leica DMIRE2 equipped with a TCS SP2 scanner, Wetzlar, Germany) in SSC–TW20 buffer solution (pH 7.0). Specifically, epifluorescence micrographs were taken with a 10 × objective under standard green (U-N31001) and red (U-N31002) filter sets (Chroma Technology Corp., Rockingham, VT) for the fluorescently labeled and the R-PE conjugated microspheres, respectively. Confocal micrographs were taken with a 20 × objective at 488 nm and 543 nm excitation for the fluorescently labeled and the R-PE conjugated microspheres, respectively. Fluorescence intensities of the microspheres were analyzed with the image analysis software ImageJ [39], and averaged for at least five microspheres per each condition. For scanning electron microscopy (SEM) analysis, the as-prepared microspheres were washed 3 times with DI water containing 0.5% v/v TW20 and 2 times with DI water in order to avoid formation of salts from the buffer solution during drying process. The microspheres were freeze-dried for 24 h in a lyophilizer (Labconco Corp., Kansas City, MO). The lyophilized microspheres were then placed on a stub and coated with a thin gold–palladium layer using a sputter coater (The 108 Auto Sputter Coater, Ted Pella, Inc., Redding, CA), and analyzed with a scanning electron microscope operating at 5 kV (JEOL 5910, JEOL USA, Inc., Peabody, MA).

3. Results and discussion

3.1. Consistent fabrication of uniform hydrogel microspheres at varying contents of the porogen with the micromolding-based technique

We first demonstrate that our simple micromolding-based technique allows for consistent fabrication of highly uniform hydrogel microspheres at varying compositions of prepolymer solution containing short PEG porogen (PEG600). Specifically, as shown in the scheme of Fig. 1(a), the cross-shaped PDMS micromolds are filled with photocurable prepolymer solution containing aqueous mixture of PEGDA, PEG600 and chitosan. The addition of wetting fluid (*N*-hexadecane with photoinitiator, PI) onto the filled micromolds induces formation of uniform prepolymer droplets by surface tension between the interface of the hydrophilic prepolymer solution and the hydrophobic wetting fluid (leftmost bright-field micrograph in the bottom row of Fig. 1(a)). Simple photo-induced polymerization with a hand-held UV lamp (365 nm) leads the droplets to form uniform microspheres (middle micrograph). Specifically, the UV light induces formation of highly reactive radicals from the PI via photolysis, and the radicals react with the acrylate groups of PEGDA generating chain-initiating radicals [43]. Successive addition of PEGDA then takes place by the chain-initiating radicals, leading to rapid growth and crosslinking of polymer chains and thus formation of the hydrogel networks. During this propagation step, chitosan molecules can be incorporated with the networks in a stable manner by the reaction between acrylates of PEGDA and primary amines of chitosan [18,25]. Note that the incorporated chitosan still retains majority of its chemical functionality from remaining primary amines due to low reaction efficiency between the acrylates and amines [44–46]. Meanwhile, the crosslinked PEG chains and PEG600 create excluded volume by phase separation (i.e., PIPS) during the polymerization, and leads to formation of macropores in the microspheres upon washing (further discussed in the following sections).

We first examined the uniformity and water content of the microspheres prepared with varying compositions of the prepolymer solution (i.e., 10 v/v% and 15 v/v% PEGDA with 0–30 v/v% PEG600) via simple microscopic image analysis and drying experiments. As shown in the table of Fig. 1(b), microspheres fabricated with either 10% or 15% PEGDA and varying PEG600 contents all showed uniform wet and dry diameters, as indicated by consistently small standard deviations from minimum 30 samples examined per condition and three different directions in diameter measured per sample. This result illustrates that our simple micromolding-based technique enables fabrication of highly uniform microspheres in a consistent manner. The volumetric swelling ratios and water contents calculated from these measurements show similarly high values under varying PEGDA and PEG600 content conditions, with microspheres prepared with 15% PEGDA showing relatively lower swelling ratios rising from higher PEGDA content and more efficient polymerization than the ones from 10% PEGDA in general [21,26]. There exists a modest trend of increasing swelling ratio (4.2 to 4.9) and water content (76% to 80%) with increasing PEG600 contents for the 15% PEGDA conditions.

In short summary, the results in Fig. 1 show that our simple micromolding technique enables reliable fabrication of microspheres with consistent dimensions and high water content from various prepolymer compositions (i.e., PEGDA and PEG600 contents).

3.2. Effect of porogen contents on distribution of chitosan within microspheres

Next, we carried out simple fluorescent labeling of the as-prepared microspheres with amine reactive fluorescent markers to examine distribution of reactive primary amine groups from chitosan within the microspheres (Fig. 2). As shown in the schematic diagram, the unshared electron pair of the primary amine group of chitosan and the electron-deficient carbonyl carbon of the NHS ester derivative of fluorescein (NHS-fluorescein) undergoes acyl substitution reaction to form a stable amide linkage, enabling simple visualization of the presence, reactivity and distribution of chitosan [19].

First, the bright-field images of all the as-prepared microspheres with varying PEGDA and PEG contents (leftmost columns) show uniform sizes as in Fig. 1(b), while increasing PEG content leads to darker appearances for both 10% and 15% PEGDA cases presumably due to the formation of macropores [47,48]. Next, the epifluorescence images (top view, middle columns) show distinct fluorescence on the microspheres unlike negligible fluorescence on the microspheres without chitosan (Supplementary Data, Fig. S1), indicating successful incorporation of chitosan with the microspheres and specific nature of the reaction. Importantly, the fluorescent labeling results show striking differences in the distribution and intensity of fluorescence (i.e., chitosan) in the conditions examined here. For the 10% PEGDA case, the chitosan moieties appear to be distributed uniformly throughout the microspheres prepared without PEG600 as consistent with our previous report [26]. The addition of 10% PEG600 does not appear to significantly alter the chitosan distribution unlike 20% PEG600 condition, where high fluorescence on a small region in the microsphere core indicates dense chitosan. Meanwhile, the addition of 30% PEG600 leads to uniform yet lower fluorescence intensity compared to other conditions. Considering small size of the fluorescein marker used here (estimated diameter $d \approx 0.7$ nm, MW 473.4 Da) [49] and thus its minimal mass transfer limitation into the microspheres [18,26,47], the low fluorescence intensity is attributed to lower chitosan incorporation efficiency. This result is attributed to interference of

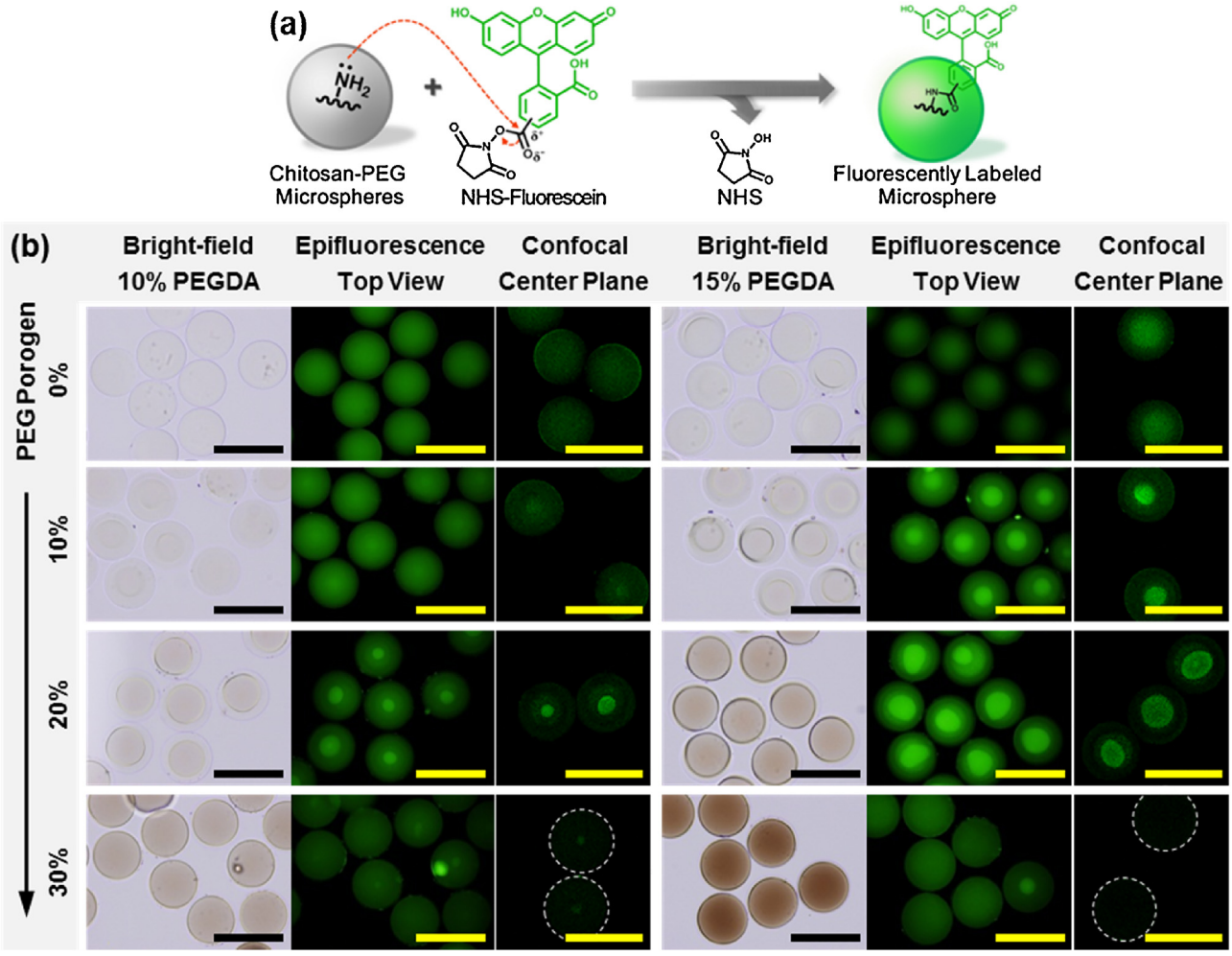

Fig. 2. Fluorescence labeling of chitosan–PEG microspheres via amidation reaction. (a) Schematic diagram describing the amidation reaction between primary amine in the microspheres and NHS ester group of the NHS-fluorescein molecules. (b) Bright-field, epifluorescence and confocal micrographs of microspheres prepared with varying compositions of prepolymer solution upon fluorescence labeling. All scale bars represent 200 μm.

polymerization reaction by high PEG600 content [21]. Next, the microspheres prepared with 15% PEGDA show brighter fluorescence (thus denser chitosan) in the core region in general, unlike the 10% PEGDA microspheres. Chitosan density appears to increase with increasing PEG600 concentration from 0% to 20%. As similar to the 10% PEGDA case, the 15% PEGDA microspheres prepared with 30% PEG600 show low fluorescence, again presumably due to interference of chitosan incorporation by high PEG600 content. Finally, the confocal microscopy images taken at the center plane of the fluorescently labeled microspheres (rightmost columns) correlate well with and further confirm the chitosan distribution shown in the epifluorescence images. Notably, the results in Fig. 2 indicate tunable chitosan distribution (i.e., conjugation handles) in the microspheres via simple addition of PEG600 and adjustment of prepolymer compositions, which may enable programmable biomolecule conjugation. In the meantime, higher PEGDA concentration conditions (≥20%) show minimal change in the chitosan distribution even with the addition of the same PEG600 contents examined here (data not shown). We will thus focus on the prepolymer compositions examined here for the protein conjugation experiment in the following sections (i.e., 10% and 15% PEGDA, 0–30% PEG600).

In sum, the fluorescent labeling results in Fig. 2 show that simple addition of PEG600 porogen can dramatically change the incorporation and distribution of chitosan in the microspheres.

3.3. *Macroporous hydrogel networks formed by porogen: improved protein penetration into the microspheres*

We then examined the network structures of the microspheres in more detail by conjugating a red fluorescent protein R-phycoerythrin (R-PE), as shown in Fig. 3. R-PE is a good model protein for protein conjugation studies due to its highly bright fluorescence and large size (240 kDa, hydrodynamic diameter $d_h \approx 11.2$ nm) similar to antibodies (IgG, 150 kDa, $d_h \approx 11$ nm) that are commonly utilized as biomolecular probes. To conjugate the R-PEs with the microspheres, we utilized a rapid and bioorthogonal tetrazine–*trans*-cyclooctene (Tz–TCO) ligation reaction as shown in the schematic diagram of Fig. 3 due to its high yield and stability of each functional group (i.e., Tz and TCO) in the aqueous solution, which makes it an efficient conjugation scheme. Specifically, the microspheres prepared with varying PEGDA and PEG600 contents were activated with Tz molecules via amidation reaction using NHS ester derivative of Tz. The Tz-activated microspheres were then incubated with TCO-modified R-PEs for 24 h, and analyzed via bright-field and fluorescence microscopy.

The bright-field micrographs of the Tz-activated microspheres under all the prepolymer composition conditions show bright red color upon incubation with TCO-modified R-PEs (left columns, Fig. 3) unlike microspheres without Tz-activation (Fig. S2). This result indicates selective conjugation of R-PEs through the

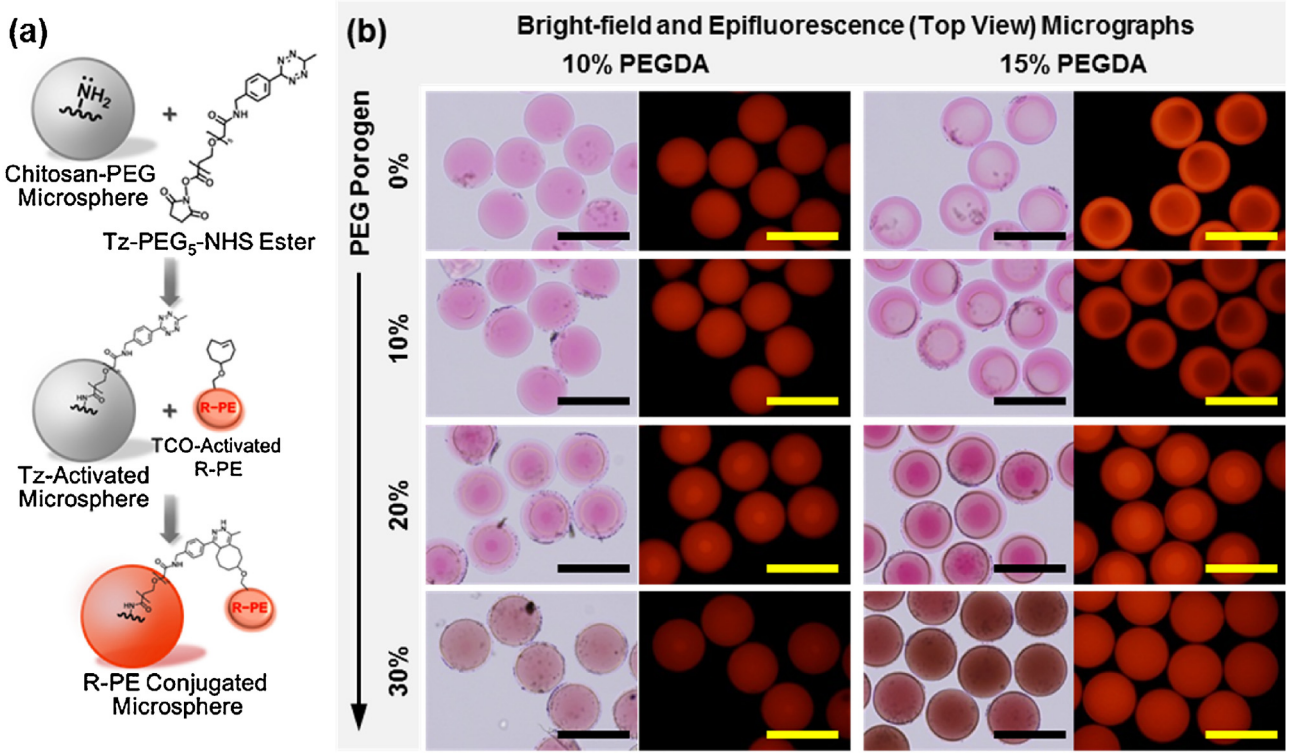

Fig. 3. R-PE conjugation with the microspheres. (a) Schematic diagram illustrating R-PE conjugation with the microspheres through Tz–TCO ligation reaction. (b) Bright-field and epifluorescence micrographs of the microspheres prepared with varying compositions of prepolymer solution upon conjugation reaction. All scale bars represent 200 μm. (For interpretation of the references to color in text, the reader is referred to the web version of this article.)

biorthogonal Tz–TCO reaction and high R-PE conjugation capacity of the microspheres. Importantly, the microspheres show different color (i.e., R-PE conjugation) profiles depending on the composition of the prepolymer solution. Specifically, the 10% PEGDA microspheres prepared with 20% PEG600 show brighter red color in the core region unlike uniform color profile of other PEG600 cases (i.e., 0%, 10%, and 30%). For the 15% PEGDA microspheres, 0% and 10% PEG600 cases show brighter red color near the sphere surfaces, while 20% and 30% PEG600 cases show denser color around the microsphere centers and uniform color profile throughout the microspheres, respectively.

The epifluorescence microscopy results (right columns, Fig. 3) further confirm and clearly show different R-PE conjugation profiles depending on the composition of the prepolymer solution. First, the 10% PEGDA microspheres show consistent red fluorescence profiles for the 0%, 10% and 30% PEG600 content, and denser fluorescence near the centers for the 20% PEG600 content conditions, consistent with the chitosan distribution (via NHS-fluorescein labeling) shown in Fig. 2. Considering large size of the R-PE (d_h≈11.2 nm), this result suggests that mesh sizes of the 10% PEGDA microspheres are large enough for the R-PEs to penetrate into the microspheres and be conjugated even in the core region within 24 h. Next, 15% PEGDA microspheres show higher fluorescence intensity in the shell region for 0% and 10% PEG600. Compared to the dense chitosan distribution around the core region of the same microspheres (Fig. 2), this result suggests hindered R-PE penetration due to small mesh sizes. Meanwhile, the thickness of the bright shell region increases with increasing PEG600 content up to 10%, and the microspheres prepared with 20% and 30% PEG600 show consistent fluorescence profile with the chitosan distribution suggesting full penetration of the R-PEs. Thus, these results reveal tunable mesh sizes and 3D structures of the hydrogel networks simply by adjusting PEG600 content in the 15% PEGDA prepolymer solution. Lastly, both 10% and 15% PEGDA microspheres with 30% PEG600 show slightly lower fluorescence intensity; we attribute this to lower chitosan incorporation efficiency resulting from high content of inert PEG600. Meanwhile, the microspheres prepared with the same conditions as in Fig. 3 yet without Tz-activation show negligible fluorescence, indicating minimal nonspecific binding and selective conjugation of the R-PEs via the Tz–TCO reaction (Fig. S2).

In short summary, the protein conjugation results in Fig. 3 indicate macroporous network structures with a diverse range of 3D network structures via simple tuning of the synthesis conditions (i.e. PEGDA and PEG600 contents).

3.4. *Effect of porogen contents on network structures of hydrogel microspheres*

Next, we carried out more in-depth examination of the 3D network structures of the microspheres via confocal microscopy on the R-PE-conjugated microspheres as shown in Fig. 4. In addition, the network structures were further analyzed via SEM on lyophilized microspheres prior to R-PE conjugation.

First, confocal micrographs at the center plane of the microspheres (Fig. 4, left columns) show R-PE conjugation profiles throughout the microspheres, allowing for deeper understanding of the network structures (i.e., top vs. cross-sectional view of the R-PE conjugated microspheres). The 10% PEGDA cases show uniform fluorescence distributions throughout the microspheres prepared with 0, 10 and 30% PEG600, and brighter fluorescence around the cores of the microspheres prepared with 20% PEG600, consistent with the chitosan distribution in Fig. 2. This result indicates again the formation of large pores that enables complete R-PE penetration into the microspheres. Next, the microspheres prepared with 15% PEGDA show varying R-PE conjugation profiles depending on the PEG600 contents. Specifically, the 0% and 10% PEG600 cases show brighter fluorescence in the shell regions and negligible fluo-

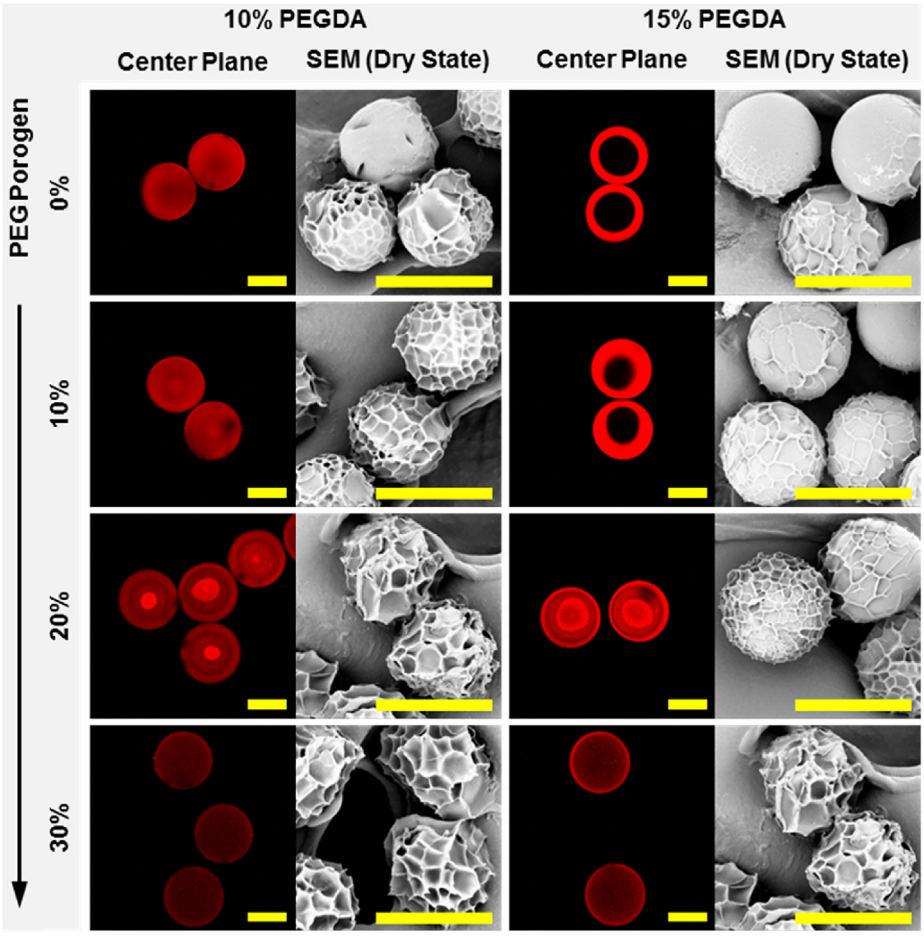

Fig. 4. Three dimensional network structures of the microspheres. Representative confocal micrographs and SEM images of R-PE conjugated and lyophilized microspheres, respectively. All scale bars represent 100 μm.

rescence at the cores, indicating hindered penetration of the R-PEs into the microspheres (i.e., incomplete penetration even after 24 h incubation) due to small mesh sizes. Importantly, thickness of the bright shell layer increases with increasing PEG600 content up to 10%, and the addition of higher PEG600 contents (i.e., 20% and 30%) allows for complete R-PE penetration (i.e., red fluorescence in the cores). This result reveals again tunable mesh sizes and formation of macroporous network structures by simple addition of PEG600 porogen in the prepolymer solutions. Meanwhile, higher PEGDA concentration conditions (above 20%) show minimal increase in the R-PE penetration even with the addition of the PEG600 (data not shown).

Next, the SEM images of lyophilized microspheres (Fig. 4, right columns) support the trends in the R-PE conjugation profiles and formation of the macroporous network. Specifically, microspheres prepared with 10% PEG show rough surfaces with "wrinkles" in all PEG600 content cases. We attribute these wrinkled morphologies to collapsed hydrogel networks during lyophilization due to macroporous network structures that allowed for complete penetration of R-PEs shown in the confocal images. The wrinkled regions and holes on the microspheres become larger with higher PEG600 contents, which suggest decrease in polymer content and crosslinking possibly due to less efficient polymerization with higher PEG600 contents [21]. In the meantime, the 15% PEGDA microspheres prepared with 0% and 10% PEG600 show relatively smooth surfaces compared to those of 10% PEGDA microspheres. These smooth surfaces are attributed to relatively tight network structures resulting from relatively higher polymer content and polymerization efficiency [21,26]. For the 20% and 30% PEG600 cases, the microspheres show wrinkled morphologies and rough surfaces similar to the 10% PEGDA microspheres, suggesting macroporous network formation by increasing PEG600 contents. Overall, the transition from smooth to wrinkled morphologies of the 15% PEGDA microspheres corresponds to increase in the R-PE penetration depth shown in the confocal images, and supports tunable mesh sizes of the network structures by simple addition of PEG600.

In short summary, the confocal microscopy and SEM results in Fig. 4 show macroporous nature of the microspheres by using PEG600 porogen, leading to various 3D network structures and distributions of the functional groups (i.e., chitosan) ranging from uniformly porous, center-concentrated and variable shell layers.

3.5. *Effect of hydrogel network structures on protein conjugation kinetics*

Finally, we carried out thorough examination of the effect of the network structures on the kinetic behavior of the protein conjugation using the R-PE and Tz–TCO ligation reaction, as shown in Fig. 5. For this, the microspheres prepared with varying prepolymer compositions were activated with Tz molecules (Schematic diagram, Fig. 3). We then incubated Tz-activated microspheres with 2 μM TCO-modified R-PE, and measured total fluorescence intensities of the microspheres at varying time points for the 24 h reaction period. Note, the very rapid nature of the Tz–TCO reaction (i.e., $k = 820\ M^{-1}s^{-1}$) [50] allows the R-PE conjugation to represent diffusion of the R-PEs in the microsphere in a diffusion–reaction coupled

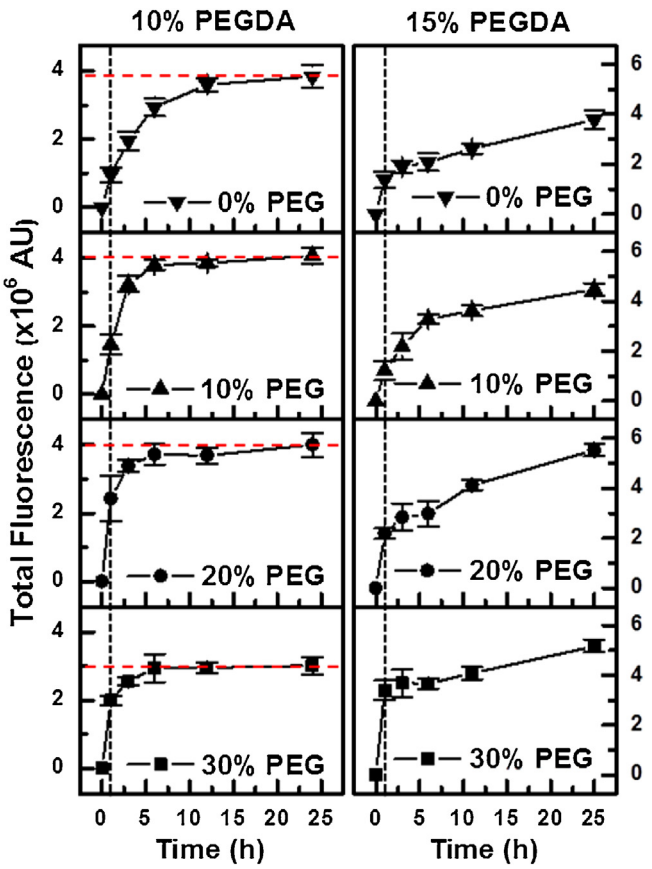

Fig. 5. R-PE conjugation kinetics with the microspheres. Black vertical and red horizontal dashed lines represent 1 h reaction and maximum conjugation capacity per each condition, respectively. (For interpretation of the references to colour in this figure legend, the reader is referred to the web version of this article).

mass transfer system [21,47]. In other words, the observed fluorescence intensity is the result of R-PE penetration by diffusion, since the conjugation occurs as soon as the TCO-modified R-PEs reach Tz sites even at very low concentration.

First, the total fluorescence intensity of the 10% PEGDA microspheres prepared without the PEG600 porogen (the top graph of the left column in Fig. 5) gradually increases with time throughout the 24 h reaction period, which is consistent with our recent study [26]. Specifically, the total fluorescence intensity reaches maximum value upon 24 h reaction (i.e., conjugation completion, horizontal dashed line), with 25% and 75% of the conjugation completion upon 1 h (vertical dashed line) and 6 h reaction, respectively. While the R-PE conjugation results (i.e., complete penetration of the R-PEs) indicate macroporous network structures of the 10% PEGDA microspheres, the apparent conjugation kinetics appears slow possibly due to similar or slightly larger mesh size of the microspheres compared to the R-PE size [26,47]. The apparent R-PE conjugation kinetics is considerably improved by using the PEG600 porogen, reaching 36%, 61% and 66% of the conjugation completion upon 1 h reaction with 10%, 20% and 30% PEG600, respectively, and near-complete conjugation within 6 h. We attribute this improvement in the conjugation kinetics to further increase in the mesh size of the hydrogel network structure with the PEG600 porogen, which correlates well with the SEM results (i.e., more wrinkled microsphere surfaces with higher PEG600 contents, Fig. 4). In particular, the 10% PEGDA microspheres with 30% PEG600 show significant improvement in the apparent conjugation kinetics (i.e., 67% of conjugation completion within 1 h) compared to hydrogel microspheres without mesh size control, showing roughly 60% of R-PE conjugation completion upon at least 3 h reaction in our recent report [26]. Meanwhile, the apparent conjugation kinetics shown here is comparable to that with our recently reported porosity-tuned polyacrylamide (PAAm) microspheres, whose estimated pore size is roughly 39 nm [47].

The 15% PEGDA microspheres also show improvement in the apparent conjugation kinetics with the PEG600 porogen, again suggesting an increase in the mesh sizes of the microspheres by the PEG600 porogen. However, the 15% PEGDA microspheres show relatively slow conjugation kinetics (i.e., still approaching conjugation completion even upon 24 h reaction) compared to that of the 10% PEGDA ones. We attribute this to smaller mesh sizes resulting from more polymer contents and degree of crosslinking in the 15% PEGDA microspheres. In the meantime, small error bars for every condition in the fluorescence intensity plots further indicate consistency of our fabrication-conjugation scheme.

Finally, we also examined the effect of incubation time between the droplet formation and the UV-induced polymerization on the apparent R-PE conjugation kinetics in order to further elucidate the role of PEG600 porogen, while our recent study had already shown PIPS-based core-shell formation by PEGDA during polymerization [26]. Briefly, the microspheres prepared with 15% PEGDA, 20% PEG600 and 0.5% chitosan showed no difference in either conjugation kinetics or 3D structures when the incubation time was varied from 0 h to 24 h between droplet formation and polymerization (data not shown). This result indicates that the improved protein conjugation kinetics as well as various 3D network structures observed with varying PEG600 contents stem from during, not prior to, the polymerization step.

This improved protein conjugation kinetic behavior with PEG600 porogen is consistent with the static binding assay results reported by the Doyle group, where full-length mRNA's with estimated radii of gyration from 7 to 11 nm were successfully captured in PEGDA-based hydrogel microparticles prepared with 20% PEG600 but not with PEG200, without significant deterioration of binding capacity (i.e. inhibition of co-polymerization) [7]. Notably, our results in Fig. 5 not only show the progressive improvement in the apparent protein conjugation kinetics behavior but also diminishing capacity at higher PEG600 content. Since PEG600 has substantially smaller molecular weight and volume compared to the observed protein and mesh sizes yet acts as inert additive and rinsed away upon polymerization, pinpointing the precise mechanism on the modulation of mesh sizes has proven challenging in our studies. Finally, our attempt at theoretical calculation of the observed macropore formation phenomena using Hildebrand and Hansen solubility parameters proved unsuccessful due to the aqueous nature of the polymerization environment presenting large number of unknown variables. Further in-depth investigation on the fundamental role and mechanism of PEG porogens in aqueous fabrication conditions is thus much needed.

In summary, the results of substantially improved apparent protein conjugation kinetics in Fig. 5 clearly indicate tunable hydrogel network structures and macropore formation by simple modification of prepolymer compositions with the PEG600 porogen.

4. Conclusions

In this report, we demonstrated a facile approach to manufacture highly uniform and chemically reactive hydrogel microspheres with tunable and macroporous 3D networks. Specifically, highly monodisperse PEG-based hydrogel microspheres were fabricated with a simple micromolding-based technique using surface tension-induced droplet formation followed by photo-induced radical polymerization. Short chain chitosan incorporated by simple mixing in the prepolymer solution provided abundant chemi-

cal functionality that yielded a wide range of distribution from uniform, core-shell to center-condensed locations. Its highly nucleophilic nature should thus make chitosan a potent biofabrication modality in the fabrication of functional hydrogel materials in general. Mesh sizes, chitosan distribution and 3D network structures of the microspheres were readily tuned by simple addition of inert porogen, PEG600. First, fluorescent labeling study using amidation reaction showed chemical reactivity of the microspheres and controlled distribution of chitosan (i.e., uniform and core-shell) within the microspheres depending on PEG600 content in the prepolymer solution. Next, R-PE conjugation studies using Tz–TCO ligation reaction revealed controlled mesh sizes by adjusting PEG600 content, leading to formation of macroporous network structures that allows for complete penetration of the R-Pes. Analysis of R-PE conjugation kinetics supported tunable mesh sizes of the microspheres with PEG600; enhanced R-PE penetration and conjugation by increasing PEG600 content (i.e., for 10% PEGDA microspheres, 36%, 61% and 66% of the conjugation completion upon 1 h reaction with 10%, 20% and 30% PEG600, respectively) compared to the microspheres prepared without the porogen (i.e., 25% of the conjugation completion upon 1 h reaction). SEM analysis results further suggested macroporous network structures of the microspheres, showing wrinkled morphologies that result from collapsed polymer networks upon lyophilization. Finally, the highly rapid conjugation kinetics results clearly indicated formation of macroporous networks that yielded over 60% reaction completion within 1 h, showing potential for utility in rapid biosensing and diagnostic applications. Overall, these results illustrate simplicity and robustness of our approach to readily modulate the mesh structures and to control the 3D network structures of the hydrogel microspheres such as mesh sizes and distribution of chitosan moieties by simple addition of inert short-chain PEG additives. We thus anticipate that our approach shown in this report offers design principles and promising routes to construct functional microspheres with diverse 3D hydrogel network structures such as core-shell like structures, enabling manufacture of potent biofunctionalized hydrogel materials toward biosensing and medical diagnostics applications.

Acknowledgments

We thank Mr. John H. Abel for helpful discussion and feedback on the manuscript, and Mr. Eric Y. Liu for carrying out the incubation time study. We gratefully acknowledge partial financial support by the U.S. National Science Foundation (Grant # CBET-1703547), the National Research Foundation of Korea (NRF) by the Korea government (MSIT) (No. NRF-2017R1C1B2006237), and Global Research Laboratory (GRL) Program through NRF and ICT (NRF-2015K1A1A2033054).

Appendix A. Supplementary data

Supplementary material related to this article can be found, in the online version, at doi:https://doi.org/10.1016/j.bej.2018.04.012.

References

[1] D. Dendukuri, P.S. Doyle, The synthesis and assembly of polymeric microparticles using microfluidics, Adv. Mater. 21 (2009) 4071–4086.
[2] Y. Duenas, J. Lee, S. Jung, H. Yi, Multiplexed hydrogel microparticle suspension arrays for facile ribosomal RNA integrity assays, Biotechnol. Bioprocess Eng. 20 (2015) 956–964.
[3] J.H. Kim, T.Y. Jeon, T.M. Choi, T.S. Shim, S.-H. Kim, S.-M. Yang, Droplet microfluidics for producing functional microparticles, Langmuir 30 (2014) 1473–1488.
[4] G.C. Le Goff, R.L. Srinivas, W.A. Hill, P.S. Doyle, Hydrogel microparticles for biosensing, Eur. Polym. J. 72 (2015) 386–412.
[5] A.A. Ellington, I.J. Kullo, K.R. Bailey, G.G. Klee, Antibody-based protein multiplex platforms: technical and operational challenges, Clin. Chem. 56 (2010) 186–193.
[6] D.C. Pregibon, M. Toner, P.S. Doyle, Multifunctional encoded particles for high-throughput biomolecule analysis, Science 315 (2007) 1393–1396.
[7] N.W. Choi, J. Kim, S.C. Chapin, T. Duong, E. Donohue, P. Pandey, W. Broom, W.A. Hill, P.S. Doyle, Multiplexed detection of mRNA using porosity-tuned hydrogel microparticles, Anal. Chem. 84 (2012) 9370–9378.
[8] D.C. Appleyard, S.C. Chapin, P.S. Doyle, Multiplexed protein quantification with barcoded hydrogel microparticles, Anal. Chem. 83 (2011) 193–199.
[9] J.E. Meiring, M.J. Schmid, S.M. Grayson, B.M. Rathsack, D.M. Johnson, R. Kirby, R. Kannappan, K. Manthiram, B. Hsia, Z.L. Hogan, A.D. Ellington, M.V. Pishko, C.G. Willson, Hydrogel biosensor array platform indexed by shape, Chem. Mater. 16 (2004) 5574–5580.
[10] T.J. Merkel, K.P. Herlihy, J. Nunes, R.M. Orgel, J.P. Rolland, J.M. DeSimone, Scalable, shape-specific, top-down fabrication methods for the synthesis of engineered colloidal particles, Langmuir 26 (2010) 13086–13096.
[11] C.L. Lewis, C.H. Choi, Y. Lin, C.S. Lee, H. Yi, Fabrication of uniform DNA-conjugated hydrogel microparticles via replica molding for facile nucleic acid hybridization assays, Anal. Chem. 82 (2010) 5851–5858.
[12] T.S. Shim, S.-H. Kim, S.-M. Yang, Elaborate design strategies toward novel microcarriers for controlled encapsulation and release, Part. Part. Syst. Charact. 30 (2013) 9–45.
[13] S. Seiffert, J. Thiele, A.R. Abate, D.A. Weitz, Smart microgel capsules from macromolecular precursors, J. Am. Chem. Soc. 132 (2010) 6606–6609.
[14] C.-H. Choi, H. Wang, H. Lee, J.H. Kim, L. Zhang, A. Mao, D.J. Mooney, D.A. Weitz, One-step generation of cell-laden microgels using double emulsion drops with a sacrificial ultra-thin oil Shell, Lab Chip 16 (2016) 1549–1555.
[15] D.F. Coutinho, A.F. Ahari, N.N. Kachouie, M.E. Gomes, N.M. Neves, R.L. Reis, A. Khademhosseini, An automated two-phase system for hydrogel microbead production, Biofabrication 4 (2012) 035003.
[16] K.J. Lee, J. Yoon, S. Rahmani, S. Hwang, S. Bhaskar, S. Mitragotri, J. Lahann, Spontaneous shape reconfigurations in multicompartmental microcylinders, Proc. Natl. Acad. Sci. U. S. A. 109 (2012) 16057–16062.
[17] S. Rahmani, S. Saha, H. Durmaz, A. Donini, A.C. Misra, J. Yoon, J. Lahann, Chemically orthogonal three-patch microparticles, Angew. Chem. Int. Ed. 53 (2014) 2332–2338.
[18] S. Jung, H. Yi, Facile strategy for protein conjugation with chitosan-poly(ethylene glycol) hybrid microparticle platforms via strain-promoted alkyne-azide cycloaddition (SPAAC) reaction, Biomacromolecules 14 (2013) 3892–3902.
[19] S. Jung, H. Yi, Integrated fabrication-conjugation approaches for biomolecular assembly and protein sensing with hybrid microparticle platforms and biofabrication - a focused minireview, Korean J. Chem. Eng. 32 (2015) 1713–1719.
[20] W.S. Tan, C.L. Lewis, N.E. Horelik, D.C. Pregibon, P.S. Doyle, H.M. Yi, Hierarchical assembly of viral nanotemplates with encoded microparticles via nucleic acid hybridization, Langmuir 24 (2008) 12483–12488.
[21] D.C. Pregibon, P.S. Doyle, Optimization of encoded hydrogel particles for nucleic acid quantification, Anal. Chem. 81 (2009) 4873–4881.
[22] W. Kusnezow, J.D. Hoheisel, Solid supports for microarray immunoassays, J. Mol. Recognit. 16 (2003) 165–176.
[23] R.A. Floyd, J.M. Carney, Free-radical damage to protein and DNA - mechanisms involved and relevant observations on brain undergoing oxidative stress, Ann. Neurol. 32 (1992) S22–S27.
[24] D.I. Pattison, M.J. Davies, Actions of ultraviolet light on cellular structures, Experientia Suppl. (2006) 131–157.
[25] S. Jung, H. Yi, Fabrication of chitosan-poly(ethylene glycol) hybrid hydrogel microparticles via replica molding and its application toward facile conjugation of biomolecules, Langmuir 28 (2012) 17061–17070.
[26] S. Jung, H. Yi, Facile micromolding-based fabrication of biopolymeric-synthetic hydrogel microspheres with controlled structures for improved protein conjugation, Chem. Mater. 27 (2015) 3988–3998.
[27] M. Rinaudo, G. Pavlov, J. Desbrieres, Influence of acetic acid concentration on the solubilization of chitosan, Polymer 40 (1999) 7029–7032.
[28] P. Sorlier, A. Denuziere, C. Viton, A. Domard, Relation between the degree of acetylation and the electrostatic properties of chitin and chitosan, Biomacromolecules 2 (2001) 765–772.
[29] K.M. Varum, M.H. Ottoy, O. Smidsrod, Water-solubility of partially N-acetylated chitosans as a function of pH - effect of chemical-composition and depolymerization, Carbohydr. Polym. 25 (1994) 65–70.
[30] Y. Liu, E. Kim, R. Ghodssi, G.W. Rubloff, J.N. Culver, W.E. Bentley, G.F. Payne, Biofabrication to build the biology-device interface, Biofabrication 2 (2010) 022002.
[31] F. Pena, A. Gutierrez-Lerma, R. Quiroz-Baez, C. Arias, The role of beta-amyloid protein in synaptic function: implications for Alzheimer's disease therapy, Curr. Neuropharmacol. 4 (2006) 149–163.
[32] F. Ashall, A.M. Goate, Role of the beta-amyloid precursor protein in Alzheimer's disease, Trends. Biochem. Sci. 19 (1994) 42–46.
[33] H.M.J. Boots, J.G. Kloosterboer, C. Serbutoviez, F.J. Touwslager, Polymerization-induced phase separation.1. Conversion-phase diagrams, Macromolecules 29 (1996) 7683–7689.
[34] A.Y. Kwok, E.L. Prime, G.G. Qiao, D.H. Solomon, Synthetic Hydrogels 2. Polymerization induced phase separation in acrylamide systems, Polymer 44 (2003) 7335–7344.

[35] C.H. Choi, J.M. Jeong, S.M. Kang, C.S. Lee, J. Lee, Synthesis of monodispersed microspheres from Laplace pressure induced droplets in micromolds, Adv. Mater. 24 (2012) 5078–5082.
[36] C.H. Choi, B. Lee, J. Kim, J.O. Nam, H. Yi, C.S. Lee, Controlled fabrication of microparticles with complex 3d geometries by tunable interfacial deformation of confined polymeric fluids in 2d micromolds, ACS Appl. Mater. Interfaces 7 (2015) 11393–11401.
[37] E.Y. Liu, S. Jung, H. Yi, Improved protein conjugation with uniform, macroporous poly(acrylamide-co-acrylic acid) hydrogel microspheres via EDC/NHS chemistry, Langmuir (2016).
[38] Y. Shin, S. Han, J.S. Jeon, K. Yamamoto, I.K. Zervantonakis, R. Sudo, R.D. Kamm, S. Chung, Microfluidic assay for simultaneous culture of multiple cell types on surfaces or within hydrogels, Nat. Protoc. 7 (2012) 1247–1259.
[39] W.S. Rasband, Imagej, U. S. National Institutes of Health, Bethesda, Maryland, USA, 1997, pp. 2016.
[40] L.G. Wade, Organic Chemistry, 5th ed., Pearson Education, Upper Saddle River, NJ, 2003.
[41] G.T. Hermanson, Bioconjugate Techniques, 2nd ed., Elsevier Science, Burlington, MA, 2008.
[42] Anaspec, Inc. Home Page, 2016 (accessed 11 April 11 2016) http://www.anaspec.com/products/product.asp?id=29041.
[43] G. Odian, Principles of Polymerization, 4th ed., Wiley, Hoboken, NJ, 2004.
[44] I.M. El-Sherbiny, Synthesis, characterization and metal uptake capacity of a new carboxymethyl chitosan derivative, Eur. Polym. J. 45 (2009) 199–210.
[45] I.M. El-Sherbiny, H.D.C. Smyth, Poly(Ethylene glycol)-carboxymethyl chitosan-based pH-responsive hydrogels: photo-induced synthesis, characterization, swelling, and in vitro evaluation as potential drug carriers, Carbohydr. Res. 345 (2010) 2004–2012.
[46] M.W. Sabaa, N.A. Mohamed, R.R. Mohamed, N.M. Khalil, S.M.A. El Latif, Synthesis, characterization and antimicrobial activity of poly (N-vinyl imidazole) grafted carboxymethyl chitosan, Carbohydr. Polym. 79 (2010) 998–1005.
[47] S. Jung, J.H. Abel, J.L. Starger, H. Yi, Porosity-tuned chitosan-polyacrylamide hydrogel microspheres for improved protein conjugation, Biomacromolecules 17 (2016) 2427–2436.
[48] E. Kang, S. Jung, J.H. Abel, A. Pine, H. Yi, Shape-encoded chitosan-polyacrylamide hybrid hydrogel microparticles with controlled macroporous structures via replica molding for programmable biomacromolecular conjugation, Langmuir 32 (2016) 5394–5402.
[49] A. Cvetkovic, C. Picioreanu, A.J.J. Straathof, R. Krishna, L.A.M. van der Wielent, Relation between pore sizes of protein crystals and anisotropic solute diffusivities, J. Am. Chem. Soc. 127 (2005) 875–879.
[50] M.R. Karver, R. Weissleder, S.A. Hilderbrand, Synthesis and evaluation of a series of 1,2,4,5-Tetrazines for bioorthogonal conjugation, Bioconjugate Chem. 22 (2011) 2263–2270.